JGR Planets

RESEARCH ARTICLE
10.1029/2018JE005891

Oblique Reflections of Mars Express MARSIS Radar Signals From Ionospheric Density Structures: Raytracing Analysis

F. Němec[1], D. J. Andrews[2], D. D. Morgan[3], A. J. Kopf[3], and D. A. Gurnett[3]

[1]Faculty of Mathematics and Physics, Charles University, Prague, Czech Republic, [2]Swedish Institute of Space Physics, Uppsala, Sweden, [3]Department of Physics and Astronomy, University of Iowa, Iowa City, IA, USA

Key Points:
- Raytracing analysis is carried out to obtain realistic trajectories of oblique echoes through the ionosphere and appropriate time delays
- Initially oblique sounding signals are significantly bent, resulting in an upper limit on the propagation distance and related time delays
- The results are used to perform a detailed case study of oblique reflections observed in the Mars Express MARSIS data

Correspondence to:
F. Němec,
frantisek.nemec@gmail.com

Citation:
Němec, F., Andrews, D. J., Morgan, D. D., Kopf, A. J., & Gurnett, D. A. (2019). Oblique reflections of Mars Express MARSIS radar signals from ionospheric density structures: Raytracing analysis, *Journal of Geophysical Research: Planets*, *124*, 1177–1187. https://doi.org/10.1029/2018JE005891

Received 23 NOV 2018
Accepted 14 MAR 2019
Accepted article online 21 MAR 2019
Published online 6 MAY 2019

Abstract Mars Advanced Radar for Subsurface and Ionosphere Sounding (MARSIS) radar sounder on board the Mars Express spacecraft revealed oblique reflections coming systematically from apparently stable density structures in the Martian ionosphere. Although these were typically interpreted by assuming a straight line propagation of the sounding signal at the speed of light, the ionospheric plasma is clearly a dispersive medium. Consequently, the ray propagation paths may be significantly bent, and, moreover, the observed time delays need to be interpreted in terms of realistic group velocities of the signal propagation. We select a single particularly well-pronounced event with oblique reflections observable over a large range of signal frequencies, and we employ raytracing calculations to perform its detailed analysis. An isolated density structure responsible for the reflection of the sounding signal back to the spacecraft is assumed, and the relevant ionospheric signal propagation is properly evaluated. We show that initially oblique sounding signals get progressively more oblique during their propagation, imposing an upper threshold on the angular propagation distance between the spacecraft and the reflecting density structure, in line with the observations. Considering realistic propagation paths further allows us to explain the frequency dependence of the observed time delays and to accurately model the entire event. The obtained results are consistent with the spacecraft passing very close to a spatially limited density structure. We also show that the results obtained using realistic raytracing calculations are significantly different from the results obtained using additional simplifying assumptions.

1. Introduction

The dayside ionosphere of Mars is controlled primarily by photoionization due to the incoming solar radiation (e.g., Haider et al., 2011; Nagy et al., 2004; Withers, 2009). On the other hand, a significantly more patchy nightside ionosphere (Gurnett et al., 2008) is formed—apart from the plasma transport from the dayside (Fox et al., 1993; Němec et al., 2010)—mainly due to electron impact ionization by precipitating electrons (Lillis et al.,2009, 2011; Němec et al.2011). Although Mars does not posses any global magnetic field, localized crustal magnetic fields are at times strong enough to influence both the ionospheric plasma processes (Nielsen et al., 2007; Withers et al., 2005) and electron precipitation (Brain et al., 2007; Lillis et al., 2004; Soobiah et al., 2006). Consequently, the ionospheric plasma density at locations with strong crustal magnetic fields can be significantly different than at nearby locations with weaker crustal magnetic fields. This is in particular true for the nightside ionosphere (Němec et al., 2011; Lillis et al., 2011), but it is to some extent clearly the case also for the dayside ionosphere (Andrews et al., 2015; Dubinin et al., 2016; Němec et al., 2016).

The Mars Advanced Radar for Subsurface and Ionosphere Sounding (MARSIS) radar sounder (Gurnett et al., 2005; Picardi et al., 2004) on board the Mars Express spacecraft allows for transmitting a sounding signal pulse and measuring the time delay until its eventual arrival back to the spacecraft. It turns out that, apart from typical vertical incidence reflections characteristic for the dayside ionosphere, oblique reflections from isolated density structures in the ionosphere can be occasionally observed. In fact, most ionospheric reflections detected on the nighside are oblique (Němec et al., 2011). On the dayside, oblique reflections were shown to be associated with isolated density structures at locations with strong crustal magnetic fields (Duru et al., 2006). These density structures appear to be quite common; for example, Duru et al. (2006) identified as many as 163 events in about a half year of MARSIS data (some 700 orbits). Moreover, they are apparently

rather stable, as the oblique reflections are repeatedly observed at the same locations (Andrews et al., 2014; Mohanamanasa et al., 2018). It was suggested that their formation is likely related to a scale height increase due to the heating by precipitating electrons (Duru et al., 2016). Diéval et al. (2015) determined the spatial extents along the directions of the Mars Express tracks for which the time delays of oblique reflections from density structures were lower than the time delays of vertical reflections from the nominal ionosphere, showing them to be a few hundreds of kilometers (several degrees) large. Diéval et al. (2018) used MARSIS data at the times when the spacecraft passed over the density structures and assumed vertical reflections from a horizontally stratified ionosphere to discuss possible shapes of these density structures. However, no attempt to properly interpret the oblique reflections in terms of realistic ray trajectories in the dispersive plasma medium of the ionosphere has been performed up to now.

We use raytracing calculations of the sounding signal propagation in the ionosphere to properly account for the group velocity lower than the speed of light and the change of the propagation direction over the propagation path. A detailed analysis of a single oblique reflection event is used to demonstrate the significance of this approach for a proper interpretation of observed oblique reflections. MARSIS measurements relevant for the analyzed event are described in section 2. The related raytracing results are presented in section 3, and they are discussed in section 4. Finally, section 5 contains a summary of the main results obtained.

2. Observations

In the ionospheric sounding mode, the MARSIS radar sounder uses 160 quasi-logarithmically spaced frequencies from 0.1 to 5.5 MHz ($\Delta f/f \approx 0.02$). The duration of a single quasi-sinusoidal pulse is 91.4 μs, and it is transmitted once every 7.86 ms. After transmitting the pulse, intensities of possible reflected echoes at the frequency of the transmitted pulse are recorded in 80 equally spaced time delay bins over an interval of 7.31 ms. A complete frequency sweep takes 1.257 s, and it is repeated every 7.543 s. Detailed descriptions of the instrument were given by Jordan et al. (2009), Picardi et al. (2004), and Orosei et al. (2015). Assuming a vertical signal incidence on a horizontally stratified ionosphere with the density monotonically increasing with decreasing altitude, the measured time delays as a function of the sounding signal frequency can be used to obtain electron density profiles from the spacecraft altitude down to the altitude of the peak electron density (Morgan et al., 2013). Additionally, sounding signals propagating at initially oblique angles can be reflected by density structures in the ionosphere and eventually make it back to the spacecraft and be detected by MARSIS. Although interpreting such oblique echoes can be challenging, an important starting point is to realize that—neglecting the magnetic field effects, which is generally a good approximation in case of Mars (Němec et al., 2010)—a signal gets reflected at a location where the signal frequency f meets electron plasma frequency f_{pe} ($f = f_{pe}$). Further, in order for the sounding signal to propagate back to the spacecraft location, density isocontours at the reflection point have to be perpendicular to the signal trajectory.

We focus on the analysis of the oblique reflection event number 2 from Figure 1 of Andrews et al. (2014). A significant advantage of this event is that (i) it is a well-formed and long-lasting event, which allows us to obtain a significant amount of relevant oblique reflection data, and (ii) the spacecraft altitude at the time of observations was rather low (about 375 km), which allows for a rather accurate determination of ionospheric electron density profiles (Němec et al., 2016, 2017). The event was observed on 31 July 2006 between about 18:51:46.756 and 18:55:40.595 UT. While the spacecraft longitude was equal to about −13.5° and principally constant over the event duration, the spacecraft latitude varied from about 33° to 18°, and solar zenith angle changed from about 25° to 27°. The spacecraft altitude varied from about 340 km in the beginning of the event up to about 420 km at the end of the event.

Although our aim is to analyze oblique reflections of the MARSIS radar signal, vertical incidence reflections are still available, and they allow us to determine electron density profiles using standardized methods (Morgan et al., 2013; Němec et al., 2016). The calculated electron density profiles are depicted in Figure 1. Individual color curves correspond to electron density profiles obtained at individual MARSIS measurement times over the event duration, and their colors correspond to increasing time, blue to red. It can be seen that the scatter of the evaluated electron density profiles is quite significant, in particular at higher altitudes. This may be expected, as the variability of electron densities in the diffusion region is rather large and turbulent-like (Andrews et al., 2015; Gurnett et al., 2010). Additionally, electron densities at altitudes above about 175±23 km (horizontal solid and dashed lines in Figure 1) are typically too low to be directly detectable by the MARSIS ionospheric sounding, and they are therefore principally an interpolation between a locally

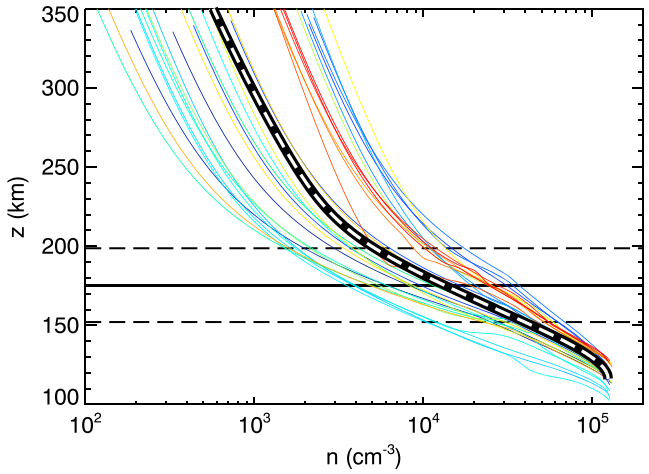

Figure 1. Electron density profiles evaluated using the Mars Advanced Radar for Subsurface and Ionosphere Sounding radar sounding data during the event duration are plotted by the color curves. The color coding corresponds to increasing time, blue to red. The solid horizontal black line marks an average altitude above which electron densities are too low to be directly detectable by the MARSIS ionospheric sounding, the dashed horizontal lines mark the respective standard deviation. A median electron density profile calculated over the event duration is plotted by the thick black/white dashed curve.

evaluated electron density and the first (lowest frequency) MARSIS radar sounding data point (Němec et al., 2017). Importantly, there appears to be no global systematic trend, and the nominal ionosphere around the location of the event can be thus in the first approximation possibly considered not to depend on the location. Although this approximation is clearly rather crude, it appears to be—given the large experimental scatter of the electron density profiles—a reasonable approach. Importantly, it allows us to obtain the electron density at any location, not just at latitudes/longitudes sampled by the spacecraft during a given path. This is crucial, as the oblique ray trajectory footprints do not need to follow the spacecraft trajectory footprints. It also ensures smooth density (refractive index) derivatives, which is desirable for the calculation. Finally, it allows for a significant simplification of the addressed problem, as in this formulation the nominal ionospheric electron density depends exclusively on the altitude.

In order to derive a single representative nominal ionospheric electron density profile for the entire event, we thus consider a median of individual electron density profiles observed during the event, and we use the fitting approach of Němec et al. (2019) to smooth and characterize the resulting profile. This resulting median profile is shown by the thick black/white dashed curve in Figure 1. It is the electron density profile that will be used in all further calculations in this paper to characterize the nominal ionosphere far from a density structure responsible for the reflection of the sounding signal. We note, however, that a different choice of the electron density profile would only marginally affect the obtained results, as long as the profile would remain reasonable, for example, even if the extreme electron density profiles from Figure 1 were used in place of the median electron density profile.

The density structure responsible for the sounding signal reflection is modeled by assuming a Gaussian density bulge; that is, the resulting isodensity contours corresponding to the structure are Gaussian-shaped rather than parallel to the planetary surface. This is achieved by shifting the nominal ionospheric electron density profile upward in altitude by a given distance. The density structure considered in our analysis is then fully characterized by its location (longitude and latitude), maximum altitude difference (in the units of kilometers), and angular extent (expressed as sigma in the units of degrees). This allows for a considerable range of resulting density configurations, while keeping the density model reasonably simple. Most importantly, given that the density bulge is assumed to be rotationally symmetric, the density model effectively depends—apart from the nominal ionospheric electron density profile and density bulge parameters—only on the angular distance from the density bulge and altitude.

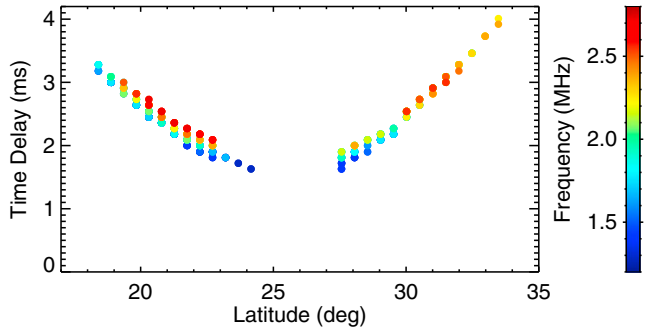

Figure 2. Time delays corresponding to the oblique ionospheric reflections detected by the MARSIS instrument during the event. The time delays are plotted as a function of the spacecraft latitude (note that the spacecraft longitude remains essentially constant over the event duration). The frequencies of the sounding signal are color coded according to the color scale on the right-hand side. Oblique reflections in the middle of the event (lowest time delays) are missing, as at those times it is difficult to distinguish them from vertical incidence echoes.

The data obtained by the MARSIS radar sounding corresponding to the oblique reflections forming the event are shown in Figure 2. Note that unlike a traditional form of color-coded plot of power spectral density, we use a higher-level data product, which benefits from the time delays of oblique reflections detected at individual sounding frequencies. These were visually determined in time delay versus time plots of detected intensities at various sounding frequencies. Figure 2 then shows the time delays corresponding to individual oblique reflections detected by MARSIS during the event as a function of the spacecraft latitude. Given that the observed shapes are most likely a result of the varying spacecraft location rather than time, and given that the spacecraft longitude remains nearly constant during the event, we believe that the spacecraft latitude is the most relevant parameter to use. Additionally, the results obtained for different sounding frequencies are distinguished by color, according to the color scale on the right-hand side. It can be seen that the observed time delays corresponding to oblique reflections are minimal roughly in

the middle of the event, and they increase toward both lower and larger latitudes. This can be interpreted as the spacecraft passing over/in the vicinity of an isolated spatially confined density structure which reflects the sounding signal (Duru et al., 2006). As the spacecraft approaches the structure, the time delays decrease, and they eventually reach a minimum when the spacecraft is closest to the reflection point. At later times, the distance of the spacecraft from the reflecting structure increases again, and so do the time delays. Note that there is an apparent data gap in the middle of the event (corresponding to the lowest time delays). This is due to the fact that at these times it is very difficult to distinguish possible oblique echoes from normal vertical incidence echoes, and no reliable experimental data can be thus obtained for this part of the event. Also note that the observed time delays corresponding to oblique reflections are generally larger for higher sounding frequencies. This is understandable, as—similarly to the vertical incidence—higher sounding frequencies make it to lower altitudes and propagate thus over larger distances before being reflected. Although for the same plasma number density the group velocity is larger for higher frequency waves, it is not enough to compensate for the longer propagation paths.

3. Raytracing Analysis

Oblique reflections from isolated density structures observed by the MARSIS instrument were typically interpreted by assuming a straight propagation at the speed of light (Duru et al., 2006; Mohanamanasa et al., 2018). Although this allows for a simple and straightforward analysis, such an approximation is obviously very rough. At the parts of the propagation paths where the electron plasma frequency approaches the sounding signal frequency, the group velocity of signal propagation is significantly lower than the speed of light, and, moreover, the wave trajectories become significantly bent. Additionally, at the spatial scales where the events are observed ($\approx 15°$, i.e., $\approx$ 1,000 km at a reference altitude of 375 km), the curvature of the planet becomes important and should be considered properly. We numerically solve Haselgrove's equations (Nickisch, 2008) to evaluate the sounding signal trajectory and time delay for a propagation in a plasma medium with a known plasma number density (electron plasma frequency). Although this ray tracing formulation is in principle 3-D, the used density model dependent only on the altitude and angular distance from a density structure responsible for the reflection allows us to effectively perform all calculations only in 2-D. Specifically, as we are interested only in the signal propagation between the density structure and the spacecraft, the two dimensions simulated in the code are altitude and angular distance from the reflecting density structure. We consider the magnetic field magnitude to be too low to have any significant effects on the wave propagation, which is generally a reasonable approximation in case of Mars (Němec et al., 2010).

In order to demonstrate some basic properties of sounding signal trajectories in the dispersive plasma of the Martian ionosphere, we first limit the analysis exclusively to the nominal ionosphere; that is, no plasma density bulge is considered at this point. Figure 3 shows example results of the raytracing analysis for the model ionosphere parameterized exclusively by altitude, which corresponds to the median electron density profile from Figure 1. The ray trajectories are plotted in the form of altitude above the planetary surface versus distance dependences. The distance is expressed in degrees, in order to remain consistent with the latitudinal variation used to characterize the spacecraft location. Waves were started at an altitude of 375 km with various initial directions. These are expressed by an angle between the initial wave direction and the vertical; that is, the initial direction of 0° corresponds to the propagation vertically down, and the initial direction of 90° corresponds to the propagation in the horizontal direction (parallel to the planetary surface). The results obtained for five different initial directions spanning from 0° to 80° are plotted to demonstrate the variability of the resulting ray paths. Having the starting altitude and the density model fixed, the ray trajectories depend—apart from the initial direction—also on the wave frequency. The results obtained for the signal frequencies of 1.2, 2.0, and 2.8 MHz are plotted by the blue, green, and red curves, respectively. Note that these frequencies were selected to roughly cover the entire frequency range where the event is observed. The solid color curves correspond to the signal trajectories before reaching the minimum altitudes, while the dotted color curves correspond to the signal trajectories after reaching the minimum altitudes. The black dashed curves correspond to straight line trajectories. However, in the used representation of altitude versus angular distance these are effectively curved due to the curvature of the planet.

Several important effects can be seen in Figure 3. For the vertical incidence as well as for other initial directions, higher-frequency signals make it to lower altitudes than lower frequency signals. The lowest altitude achievable by the ray, however, significantly depends on the initial wave vector direction Ψ, being noticeably higher for waves starting at oblique angles. In fact, assuming that the electron plasma frequency f_{pe} (i.e., for

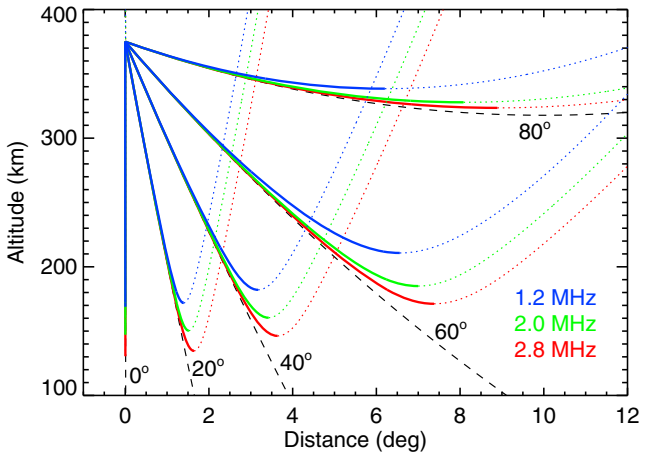

Figure 3. Results of the raytracing analysis in an example ionosphere, which assumes the same electron density profile (the one corresponding to the median electron density profile in Figure 1) at all locations. The ray altitude as a function of the distance in degrees from the starting point is plotted. The rays were started at an altitude of 375 km with various initial directions. These are marked in the figure as 0°, 20°, 40°, 60°, and 80°, with the initial direction of 0° corresponding to the propagation vertically down and the initial direction of 90° corresponding to the initial propagation in the horizontal direction (parallel to the planetary surface). The blue, green, and red curves were obtained for the signal frequencies of 1.2, 2.0, and 2.8 MHz, respectively. The parts of the trajectories before and after reaching the minimum altitudes are shown by the solid and dotted curves, respectively. The black dashed curves correspond to the straight propagation. Note that in the used representation these are effectively bent due to the curvature of the planetary surface.

a given wave frequency f also the refractive index $n = \sqrt{1-(f_{pe}/f)^2}$ depends only on the radial distance r, it is possible to obtain an analytical expression for the lowest achievable altitude. It can be shown that under such a spherical symmetry, $Q = nr\sin\Psi$ remains constant over the entire propagation path (Chen & Thorne, 2012). If we evaluate the product Q in the beginning of the ray trajectory, we can directly calculate the refractive index n at the lowest achievable altitude (where $\Psi = 90°$). Given the known electron density profile (and thus the $n(r)$ dependence), the lowest achievable altitude can be calculated. One can immediately see, in agreement with the results depicted in Figure 3, that the waves with more oblique initial angles remain at higher altitudes during the entire propagation path.

The propagation paths of waves with oblique initial angles are crucial to understand possible scenarios for their reflection from an isolated density structure. Specifically, it is unlikely—although technically feasible for specific density configurations—that the waves would get reflected back to the starting point from the upgoing parts of their propagation paths. Additionally, there would have to be an extremely large density increase to result in a wave reflection at high altitudes. In fact, in order to get reflected, a wave has to encounter a region with the plasma frequency larger than the wave frequency (as it gets reflected at a location where $f_{pe} = f$; the corresponding altitudes for a nominal ionosphere are the altitudes where the lines corresponding to the normal incidence in Figure 3 end). It thus appears reasonable to assume that the waves get reflected shortly before reaching the lowest altitude achievable during their calculated propagation paths, that is, close to the ends of the solid color curves in Figure 3.

For the sake of completeness, one should note that a sounding signal might be reflected from a density structure also during the upward part of its trajectory. However, in order for the reflected wave to propagate back to the spacecraft, the density structure in this case would have to be quite specific, with the density increasing as a function of the altitude (forming a "U-like" shape). Although such a shape of the reflecting structure cannot be excluded based on our experimental data, such density structures would be intrinsically unstable, hence likely to be short lived, and they are not further considered in the presented analysis.

Consideration of the realistic ray propagation paths results in a significant and formerly not appreciated limit on the oblique reflections. Specifically, they cannot come from an arbitrary distance, but there is a clear upper limit on this distance. Depending on the spacecraft altitude at the time of the observation, the wave frequency, and the considered electron density profile, this distance is typically less than 10° (about 650 km at a reference altitude of 375 km). This roughly corresponds to the spatial extent of the analyzed event seen in Figure 2. The maximum angular distances between the spacecraft and the lowest altitude point achievable by the sounding signal are analyzed in more detail in Figure 4a. A constant spacecraft altitude of 375 km was considered. The maximum angular distances are color coded as a function of the wave frequency and initial angle of propagation according to the color scale on the right-hand side. It can be seen that the waves with higher frequencies can generally make it to larger distances, in agreement with the results from Figure 3. However, the main controlling factor is clearly the initial propagation direction. The waves that start at more oblique angles make it to larger distances, but there is a clear threshold of about 70° in this dependence. The waves that start at too oblique directions reach the minimum altitude rather quickly, and they do not propagate too far before starting to increase in altitude again (see the blue ray path of the 1.2-MHz wave with an initial direction of 80° in Figure 3).

As the MARSIS instrument measures the time delay before the reflected waves make it back to the radar sounder, it is important to understand the behavior of time delays related to the analyzed propagation paths. These are analyzed in Figure 4b, using the same format as in Figure 4a. The dependence is rather similar as the one obtained for the maximum distances. However, there are some minor differences. These are

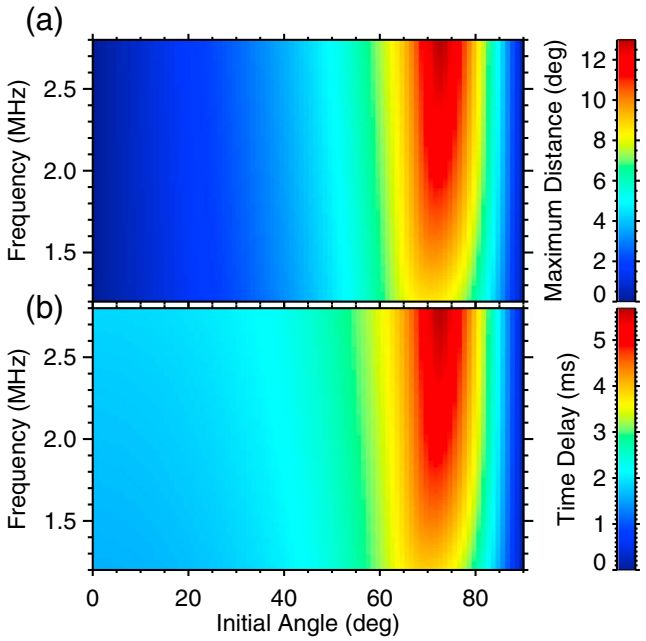

Figure 4. (a) Distance in degrees achieved by a ray before reaching the minimum altitude is color coded as a function of the wave frequency and the initial angle. The starting altitude of the ray was fixed at 375 km. The initial angle of 0° corresponds to the propagation vertically down, while the initial angle of 90° corresponds to the propagation in the horizontal direction (parallel to the planetary surface). (b) The same as (a), but the time delay corresponding to a given ray propagation is color coded instead. This was obtained as twice the time needed for the ray to reach the minimum altitude (accounting for the ray propagation to the minimum altitude and back to the spacecraft).

due to the waves of different frequencies and initial angles being reflected at different altitudes and thus propagating to the same angular distances over different lengths of the propagation paths. Additionally, the speed of propagation is not constant, but it depends on the wave frequency and the local electron plasma frequency.

The relation between the angular distances to the lowest altitude point achievable by the sounding signal and the corresponding time delays is analyzed in Figure 5. It principally corresponds to color-coded values from Figures 4a and 4b plotted one against the other, with the wave frequency color coded according to the color scale on the right-hand side. It can be seen that while the time delays at low distances increase with the sounding frequency, the time delays calculated for larger distances are basically independent of the wave frequency. This is due to fact that although the higher frequency waves propagate over a longer propagation path to get to the same angular distance, they, on the other hand, propagate with larger group velocities, and the two effects compensate for each other. This seems to be in agreement with the experimental data from Figure 2, where the time delays observed for higher frequency waves are clearly somewhat larger than for the low frequency waves, in particular close to the event center (closest to the reflection location).

In order to properly interpret the experimental data corresponding to the analyzed event, one needs to consider raytracing of sounding signals in the presence of a density bulge. For given values of the two parameters characterizing its shape and size (maximum altitude difference and angular extent) and a given spacecraft altitude, the angular distance between the density bulge location and the spacecraft location can be calculated from an observed time delay at a given sounding wave frequency. This is done by launching many different waves from a density (plasma frequency) isocontour corresponding to the sounding wave frequency, with wave normals perpendicular to the isocontour. This perpendicularity condition ensures that the waves propagating from the spacecraft to the place in question would after the reflection propagate back to the spacecraft along exactly the same trajectory. The waves are traced until they reach the spacecraft altitude, and a time delay corresponding to each of them is evaluated. Finally, the wave trajectory with the calculated time delay corresponding to half of the observed time delay (accounting for the real signal propagation from the spacecraft to the reflection location and back) is chosen as the one corresponding to the detected sounding signal. This procedure is performed for all sounding signal detections corresponding to the event, that is, for all the 508 color points from Figure 2.

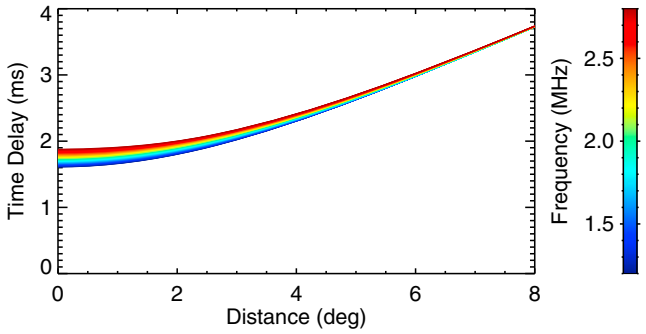

Figure 5. Time delay seen by the Mars Advanced Radar for Subsurface and Ionosphere Sounding instrument as a function of the distance in degrees to the reflection point, assuming that the signal is reflected just at the lowest altitude achievable during the propagation. The frequencies of the waves are color coded according to the color scale on the right-hand side.

Having calculated the angular distances between the spacecraft and the density bulge location at different times (spacecraft locations), the density bulge location can be determined by triangulation, that is, by finding such a location for which the sum of residual distances squared is minimal. Fixing the bulge shape, size, and location, the corresponding time delays as observed by the spacecraft can be straightforwardly calculated by applying the same procedure once again. These are then compared with the measured time delays, and the plasma bulge parameters resulting in a minimal sum of squared differences between the simulated and observed time delays are eventually selected. It is found that the best agreement is achieved for a plasma bulge with the maximum altitude difference about 170 km and angular scale size of about 0.09° located at the latitude of about 24.89° and principally just at the longitude of the spacecraft (13.48°).

Figure 6a shows the corresponding calculated angular distances between the spacecraft and the density bulge location as a function of the space-

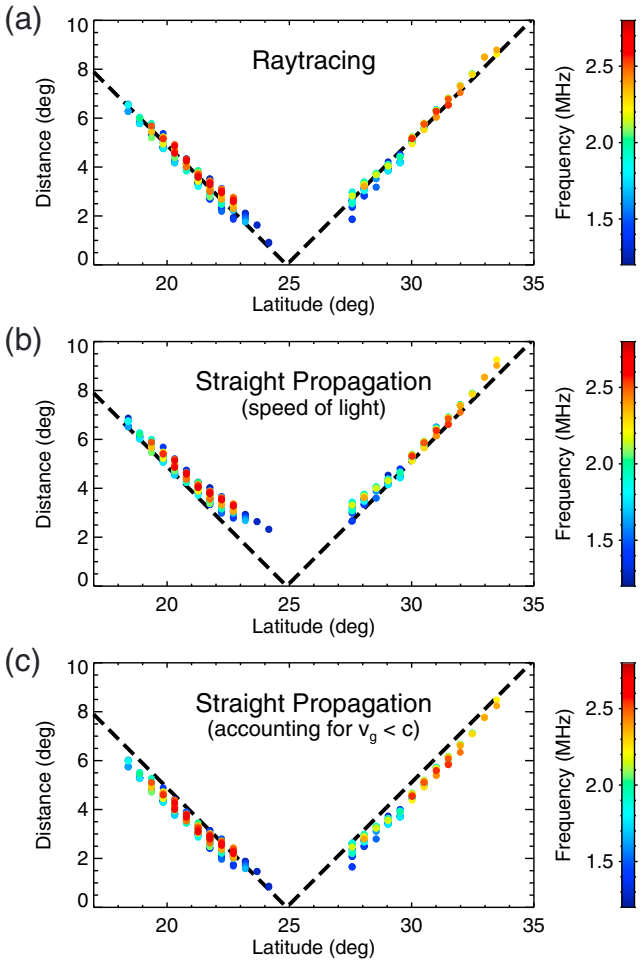

Figure 6. (a) Angular distances between the spacecraft and the reflecting plasma density bulge obtained from the raytracing analysis as a function of the spacecraft latitude are shown by the color points. The colors correspond to the wave frequencies, according to the color scale on the right-hand side. The black dashed curve, effectively degenerating into the black dashed lines, shows the angular distance between the spacecraft and the assumed plasma bulge location. (b) The same as (a), but assuming the straight propagation of the signal at the speed of light. The black dashed lines are the same as in panel (a). (c) The same as (b), but considering a realistic group velocity of the signal propagation, calculated using the model electron density profile.

craft latitude (recall that the spacecraft longitude was essentially constant during the event). The frequencies corresponding to individual data points are color coded according to the color scale on the right-hand side. The black dashed curve (which effectively degenerates into two dashed lines) shows the angular distance between the spacecraft and the assumed plasma bulge location. It can be seen that the calculation resulted in individual data points quite nicely aligned along it.

In order to demonstrate the importance of raytracing for understanding the formation of oblique reflections, Figures 6b and 6c use the same format and the same plasma bulge parameters as Figure 6a, but they were obtained assuming a straight propagation of the sounding signal. A method of calculation analogical to the method used when constructing Figure 6a was used, that is, a wave with the direction perpendicular to a given density isocontour matching the observed time delay was considered, and the appropriate angular distance between the spacecraft location and the density bulge was plotted as a function of the spacecraft latitude. Figure 6b was obtained for the straight signal propagation assuming the propagation at the speed of light, while Figure 6c was obtained for the straight signal propagation with the propagation speed properly evaluated. The dashed black lines in Figures 6b and 6c are the same as the dashed lines in Figures 6a. It can be seen that the dependences in both these—oversimplified and physically unrealistic—cases deviate

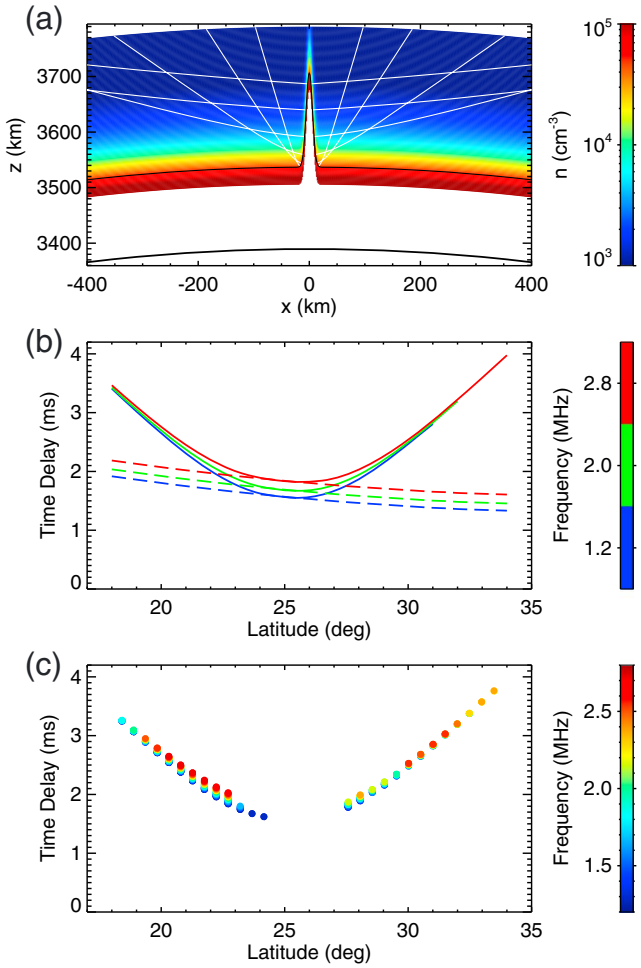

Figure 7. Overview of the situation best corresponding to the analyzed event. (a) Plasma number density close to the assumed density bulge is color coded as a function of the horizontal and vertical distance according to the color scale on the right-hand side. The black curve at the bottom of the plot corresponds to the Martian surface. The black curve approximately in the middle of the plot corresponds to a selected density isocontour (corresponding to the plasma frequency of 2 MHz). The white curves show example ray trajectories. These were calculated for the wave frequency corresponding to the plasma frequency at the selected density isocontour, and they are perpendicular to it. (b) Simulated time delays for three selected wave frequencies (1.2, 2.0, and 2.8 MHz) as a function of the spacecraft latitude are shown by the solid curves. The dashed curves show the time delays calculated for vertical reflection from a nominal ionosphere. (c) Simulated time delays corresponding to individual data points forming the event as a function of the spacecraft latitude.

substantially from the black dashed lines, demonstrating that a proper consideration of the wave propagation paths and plasma dispersion effects is crucial for a correct evaluation of oblique reflections.

Figure 7 shows an overview of the best fit scenario from Figure 6a. Figure 7a shows the model plasma number density close to the assumed plasma density bulge using the color scale on the right-hand side. Cartesian coordinates corresponding to a plane given by the spacecraft location, plasma bulge location, and the Mars center are used. The black curve at the bottom of the plot corresponds to the Martian surface. The black curve approximately in the middle of the plot represents a selected density isocontour (corresponding to the plasma frequency of 2 MHz). The white curves show example ray trajectories of 2-MHz waves, whose wave normals are perpendicular to the selected density isocontour, and which are traced up to the altitude of 400 km. The solid curves in Figure 7b show the time delays calculated for three selected wave frequencies as a function of the spacecraft latitude, taking into account the varying spacecraft altitude. The dashed curves in Figure 7b show the time delays which would correspond to a vertical reflection from a nominal ionosphere. Note that their decrease with increasing latitude is due to the decreasing altitude of the spacecraft. It can be seen that while the time delays corresponding to oblique reflections are typically larger than the

time delays corresponding to a vertical reflection from the nominal ionosphere, in a range of latitudes close to the latitude of the plasmaspheric density bulge the two time delays are well comparable. In fact, there is a latitudinal interval of about 1° where the time delays corresponding to the oblique reflections from the density bulge are lower. Looking at Figure 7a, this is understandable as the isocontour close to the plasmaspheric bulge location extends to significantly higher altitudes than in the nominal ionosphere, resulting in the sounding signal getting back to the spacecraft with shorter time delays. We note that the latitudinal interval where the time delays of oblique echoes are lower than the time delays of vertical echoes is about 5 times larger than the characteristic latitudinal extent of the plasma density bulge. Figure 7c uses the same format as Figure 2 to show the calculated time delays corresponding to individual data points. Comparing the two figures, one can see that the suggested scenario results in a very good agreement between the observed and simulated time delays. The mean absolute difference of the time delays is about 0.05ms, which is lower than the time resolution of the MARSIS instrument (about 0.09ms).

4. Discussion

The presented raytracing analysis of oblique wave propagation in the Martian ionosphere relied on a simple model of electron densities (plasma frequencies). This was based on real measured electron density profiles and parameterized exclusively by the altitude. Given the rather large experimental scatter of electron density profiles obtained by the MARSIS instrument over the area of interest, which is for most part due to a significant electron variability at high altitudes (Andrews et al., 2015; Gurnett et al., 2010) affecting in turn the entire derived electron density profiles (Morgan et al., 2013; Němec et al., 2016), this seems to be a reasonable approximation. Importantly, a change of the exact electron density model employed would result only in marginal modifications of the obtained results, with the main trends being preserved as long as the electron density model remains reasonable. Assuming that the electron plasma frequency increasing monotonically with decreasing altitude (as is generally assumed in the inversion of MARSIS ionospheric traces; see, e.g., Morgan et al., 2013), the phase speed of the wave propagation increases with decreasing altitude. This results in the wave bending "away from the normal"; that is, a wave with a nonzero initial incidence angle is progressively more and more bent during the propagation. This limits the lowest altitude achievable by the wave, as well as the maximum angular distance between the spacecraft and the reflection location.

Characterizing the density structure responsible for the oblique reflections by assuming a Gaussian-like shape of the density isocontours allowed us to eventually estimate its shape and dimensions and to determine its location. Our results strongly indicate that the density structure is spatially quite limited (spatial scales on the order of 0.1°). The maximum altitude difference of the density isocontours stemming from our calculations is higher than 100 km. We note, however, that this value clearly depends on the assumed isodensity contour shape. Given that most of the data points were obtained at larger angular separations between the spacecraft and the density structure, it is the "side of the Gaussian" which is most relevant for the analysis. In other words, should the considered shape be Gaussian-like with a more flat top, the resulting maximum altitude difference would be lower, but principally all the calculation results would remain unaffected.

Our results further suggest, in line with Duru et al. (2006), that the spacecraft passed nearly above the reflecting density structure during the event. It is thus rather surprising that the density structure was not observed in the vertical incidence data obtained by the MARSIS instrument. In particular, there appears to be no significant decrease of the detected time delays in the MARSIS data, which would be expected when the spacecraft passes just over the density structure. However, given that the separation between two consecutive MARSIS ionograms is 7.543 s, these are separated by about 0.5°. This is larger than the assumed density structure dimensions and roughly corresponds to the estimated latitudinal extent of the area where the time delays corresponding to the oblique reflections from the density structure are lower than the time delays corresponding to the vertical reflections from the nominal ionosphere. It is therefore possible that the density structure squeezed between two consecutive ionograms. It is also interesting to note that—although apparently quite stable features (Andrews et al., 2014; Mohanamanasa et al., 2018)—such density structures have not been so far observed in the local electron density data obtained by the Mars Atmosphere and Volatile EvolutioN Mission spacecraft. This seems to be consistent with very small dimensions of these structures suggested by our analysis. In this regard, one should recall that the time delays corresponding to the oblique reflections from a density structure are lower than the time delays corresponding to a vertical reflection

from the nominal ionosphere over a region significantly larger than the density structure itself; that is, these results appear to be at least roughly consistent with the observational results by Diéval et al. (2015).

5. Conclusions

We used realistic raytracing calculations to perform a detailed analysis of a well-pronounced event of oblique reflections detected by the MARSIS instrument onboard the Mars Express spacecraft. A nominal ionosphere with electron density parameterized exclusively by the altitude based on the ionospheric profiles derived from the MARSIS measurements at the times of the observations was used, and a Gaussian-shaped plasmaspheric density bulge was eventually added. We showed that initially oblique sounding signals get progressively more bent during the propagation, which imposes a clear upper threshold on an angular distance between the spacecraft and the reflecting location and the related time delays. The calculated realistic wave trajectories allow us to explain the frequency dependence of the observed time delays. The applied fitting procedure allowed us to determine the parameters of the plasmaspheric density bulge responsible for the signal reflection. It was found to be spatially significantly confined (spatial extent on the order of 0.1°), and, at the point of the closest approach, the spacecraft had to pass over its very vicinity. Finally, we demonstrated that formerly considered simplifications (straight line propagation at the speed of light) are too rough and they are not sufficient to properly evaluate the situation.

Acknowledgments
MARSIS data are available via the ESA Planetary Science Archive (http://www.rssd.esa.int/PSA). F. N. acknowledges the support of the MSMT INTER-ACTION grant LTAUSA17070.

References

Andrews, D. J., Andersson, L., Delory, G. T., Ergun, R. E., Eriksson, A. I., Fowler, C. M., & Jakosky, B. M. (2015). Ionospheric plasma density variations observed at Mars By MAVEN/LPW. *Geophysical Research Letters*, *42*, 8862–8869. https://doi.org/10.1002/2015GL065241

Andrews, D. J., André, M., Opgenoorth, H. J., Edberg, N. J. T., Diéval, C., Duru, F., & Witasse, O. (2014). Oblique reflections in the Mars Express MARSIS data set: Stable density structures in the Martian ionosphere. *Journal of Geophysical Research: Space Physics*, *119*, 3944–3960. https://doi.org/10.1002/2013JA019697

Andrews, D. J., Edberg, N. J. T., Eriksson, A. I., Gurnett, D. A., Morgan, D., Němec, F., & Opgenoorth, H. J. (2015). Control of the topside Martian ionosphere by crustal magnetic fields. *Journal of Geophysical Research: Space Physics*, *120*, 3042–3058. https://doi.org/10.1002/2014JA020703

Brain, D. A., Lillis, R. J., Mitchell, D. L., Halekas, J. S., & Lin, R. P. (2007). Electron pitch angle distributions as indicators of magnetic field topology near Mars. *Journal of Geophysical Research*, *112*, A09201. https://doi.org/10.1029/2009JA012435

Chen, L., & Thorne, R. M. (2012). Perpendicular propagation of magnetosonic waves. *Geophysical Research Letters*, *39*, L14102. https://doi.org/10.1029/2012GL052485

Diéval, C., Andrews, D. J., Morgan, D. D., Brain, D. A., & Gurnett, D. A. (2015). MARSIS remote sounding of localized density structures in the dayside Martian ionosphere: A study of controlling parameters. *Journal of Geophysical Research: Space Physics*, *120*, 8125–8145. https://doi.org/10.1002/2015JA021486

Diéval, C., Kopf, A. J., & Wild, J. A. (2018). Shapes of magnetically controlled electron density structures in the dayside Martian ionosphere. *Journal of Geophysical Research: Space Physics*, *123*, 3919–3942. https://doi.org/10.1002/2017JA025140

Dubinin, E., Fraenz, M., Andrews, D., & Morgan, D. (2016). Martian ionosphere observed by Mars Express. 1. Influence of the crustal magnetic fields. *Planetary and Space Science*, *125*, 62–75. https://doi.org/10.1016/j.pss.2016.02.004

Duru, F., Gurnett, D. A., Averkamp, T. F., Kirchner, D. L., Huff, R. L., Persoon, A. M., & Picardi, G. (2006). Magnetically controlled structures in the ionosphere of Mars. *Journal of Geophysical Research*, *111*, A12204. https://doi.org/10.1029/2006JA011975

Duru, F., Gurnett, D. A., Diéval, C., Morgan, D. D., Pisa, D., & Lundin, R. (2016). A case study of a density structure over a vertical magnetic field region in the Martian ionosphere. *Geophysical Research Letters*, *43*, 4665–4672. https://doi.org/10.1002/2016GL068686

Fox, J. L., Brannon, J. F., & Porter, H. S. (1993). Upper limits to the nightside ionosphere of Mars. *Geophysical Research Letters*, *20*(13), 1339–1342. https://doi.org/10.1029/93GL01349

Gurnett, D. A., Huff, R. L., Morgan, D. D., Persoon, A. M., Averkamp, T. F., Kirchner, D. L., & Picardi, G. (2008). An overview of radar soundings of the Martian ionosphere from the Mars Express spacecraft. *Advances in Space Research*, *41*, 1335–1346. https://doi.org/10.1016/j.asr.2007.01.062

Gurnett, D. A., Kirchner, D. L., Huff, R. L., Morgan, D. D., Persoon, A. M., Averkamp, T. F., & Picardi, G. (2005). Radar soundings of the ionosphere of Mars. *Science*, *310*, 1929–1933. https://doi.org/10.1126/science.1121868

Gurnett, D. A., Morgan, D. D., Duru, F., Akalin, F., Winningham, D., Frahm, R. A., & Barabash, S. (2010). Large density fluctuations in the Martian ionosphere as observed by the Mars Express radar sounder. *Icarus*, *206*(1), 83–94. https://doi.org/10.1016/j.icarus.2009.02.019

Haider, S. A., Mahajan, K. K., & Kallio, E. (2011). Mars ionosphere: A review of experimental results and modeling studies. *Reviews of Geophysics*, *49*, RG4001. https://doi.org/10.1029/2011RG000357

Jordan, R., Picardi, G., Plaut, J., Wheeler, K., Kirchner, D., Safaeinili, A., & Bombaci, O. (2009). The Mars Express MARSIS sounder instrument. *Planetary and Space Science*, *57*, 1975–1986. https://doi.org/10.1016/j.pss.2009.09.016

Lillis, R. J., Fillingim, M. O., & Brain, D. A. (2011). Three-dimensional structure of the Martian nightside ionosphere: Predicted rates of impact ionization from Mars Global Surveyor Magnetometer and electron reflectometer measurements of precipitating electrons. *Journal of Geophysical Research*, *116*, A12317. https://doi.org/10.1029/2011JA016982

Lillis, R. J., Fillingim, M. O., Peticolas, L. M., Brain, D. A., Lin, R. P., & Bougher, S. W. (2009). Nightside ionosphere of Mars: Modeling the effects of crustal magnetic fields and electron pitch angle distributions on electron impact ionization. *Journal of Geophysical Research*, *114*, E11009. https://doi.org/10.1029/2009JE003379

Lillis, R. J., Mitchell, D. L., Lin, R. P., Connerney, J. E. P., & Acuña, M. H. (2004). Mapping crustal magnetic fields at Mars using electron reflectometry. *Geophysical Research Letters*, *31*, L15702. https://doi.org/10.1029/2004GL020189

Mohanamanasa, P., Rao, N. V., Yaswanth, C., & Rao, S. V. B. (2018). Magnetically controlled density structures in the Martian ionosphere: Are they stably recurring? *Journal of Geophysical Research: Space Physics*, *123*, 5790–5806. https://doi.org/10.1029/2017JA024920

Morgan, D. D., Witasse, O., Nielsen, E., Gurnett, D. A., Duru, F., & Kirchner, D. L. (2013). The processing of electron density profiles from the Mars Express MARSIS topside sounder. *Radio Science*, *48*, 197–207. https://doi.org/10.1002/rds.20023

Němec, F., Morgan, D. D., Fowler, C., Kopf, A. J., Andersson, L., Gurnett, D. A., & Truhlík, V. (2017). Ionospheric electron densities at Mars: Comparison of Mars Express ionospheric sounding and MAVEN local measurements. *Journal of Geophysical Research: Space Physics*, *122*, 12,393–12,405. https://doi.org/10.1002/2017JA024629

Němec, F., Morgan, D. D., & Gurnett, D. A. (2016). On improving the accuracy of electron density profiles obtained at high altitudes by the ionospheric sounder on the Mars Express spacecraft. *Journal of Geophysical Research: Space Physics*, *121*, 10,117–10,129. https://doi.org/10.1002/2016JA023054

Němec, F., Morgan, D. D., Gurnett, D. A., & Andrews, D. J. (2016). Empirical model of the Martian dayside ionosphere: Effects of crustal magnetic fields and solar ionizing flux at higher altitudes. *Journal of Geophysical Research: Space Physics*, *121*, 1760–1771. https://doi.org/10.1002/2015JA022060

Němec, F., Morgan, D. D., Gurnett, D. A., & Brain, D. A. (2011). Areas of enhanced ionization in the deep nightside ionosphere of Mars. *Journal of Geophysical Research*, *116*, E06006. https://doi.org/10.1029/2011JE003804

Němec, F., Morgan, D. D., Gurnett, D. A., & Duru, F. (2010). Nightside ionosphere of Mars: Radar soundings by the Mars Express spacecraft. *Journal of Geophysical Research*, *115*, E12009. https://doi.org/10.1029/2010JE003663

Němec, F., Morgan, D. D., Kopf, A. J., Gurnett, D. A., Pitoňák, D., Fowler, C. M., & Andersson, L. (2019). Characterizing average electron densities in the Martian dayside upper ionosphere. *Journal of Geophysical Research: Planets*, *124*, 76–93. https://doi.org/10.1029/2018JE005849

Nagy, A. F., Winterhalter, D., Sauer, K., Cravens, T. E., Brecht, S., Mazelle, C., & Trotignon, C. B. J. G. (2004). The plasma environment of Mars. *Space Science Reviews*, *111*, 33–114. https://doi.org/10.1023/B:SPAC.0000032718.47512.92

Nickisch, L. J. (2008). Practical applications of Haselgrove's equations for HF systems. In P. Lagasse (Eds.), *The Radio Science Bulletin* (Vol. 325, pp. 36–48). Belgium URSI: Ghent University.

Nielsen, E., Fraenz, M., Zou, H., Wang, J. S., Gurnett, D. A., Kirchner, D. L., & Lundin, R. (2007). Local plasma processes and enhanced electron densities in the lower ionosphere in magnetic cusp regions on Mars. *Planetary and Space Science*, *55*, 2164–2172. https://doi.org/10.1016/j.pss.2007.07.003

Orosei, R., Jordan, R. L., Morgan, D. D., Cartacci, M., Cicchetti, A., Duru, F., & Picardi, G. (2015). Mars Advanced Radar for Subsurface and Ionospheric Sounding (MARSIS) after nine years of operation: A summary. *Planetary and Space Science*, *112*, 98–114. https://doi.org/ 10.1016/j.pss.2014.07.010

Picardi, G., Biccari, D., Seu, R., Plaut, J., Johnson, W. T. K., Safaeinili, R. L. J. A., & Zampolini, E. (2004). MARSIS: Mars Advanced Radar for Subsurface and Ionosphere Sounding. In A. Wilson, & A. Chicarro (Eds.), *Mars Express: The scientific payload* (Vol. 1240, pp. 51–69). Netherlands: ESA Publications Division.

Soobiah, Y., Coates, A. J., Linder, D. R., Kataria, D. O., Winningham, J. D., Frahm, R. A., & Dierker, C. (2006). Observations of magnetic anomaly signatures in Mars Express ASPERA-3 ELS data. *Icarus*, *1182*, 396–405. https://doi.org/10.1016/j.icarus.2005.10.034

Withers, P. (2009). A review of observed variability in the dayside ionosphere of Mars. *Advances in Space Research*, *44*, 277–3078. https://doi.org/10.1016/j.asr.2009.04.027

Withers, P., Mendillo, M., Rishbeth, H., Hinson, D. P., & Arkani-Hamed, J. (2005). Ionospheric characteristics above Martian crustal magnetic anomalies. *Geophysical Research Letters*, *32*, L16204. https://doi.org/10.1029/2005GL023483